Bacterial infection drives trained immunity through epigenetic remodeling of epithelial stem cells

Scott Hultgren (hultgren@wusm.wustl.edu)
Department of Molecular Microbiology and Center for Women's Infectious Disease Research, Washington University School of Medicine

Seongmi Russell
Washington University in St Louis https://orcid.org/0000-0003-2012-4492

Hyung Joo Lee
Pin Therapeutics, Inc. https://orcid.org/0000-0002-7030-5390

Benjamin Olson
Washington University School of Medicine https://orcid.org/0000-0002-5440-1315

Jonathan Livny
The Broad Institute of Massachusetts Institute of Technology and Harvard University
https://orcid.org/0000-0001-6589-3020

Valerie O'Brien
Fred Hutchinson Cancer Research Center, Human Biology Division

Lu Yu
Washington University School of Medicine

Elisha Roberson
Department of Genetics, Washington University School of Medicine

Shady Estfanous
Department of Microbial Infection and Immunity, Infectious Diseases Institute, Ohio State University

Amal Amer
Department of Microbial Infection and Immunity, Infectious Diseases Institute, Ohio State University

Marco Colonna
Washington University School of Medicine https://orcid.org/0000-0001-5222-4987

Thaddeus Stappenbeck
Cleveland Clinic

Ting Wang
Washington University School of Medicine https://orcid.org/0000-0002-6800-242X

Thomas Hannan
Department of Pathology and Immunology, Washington University School of Medicine, St Louis, United States https://orcid.org/0000-0003-0498-8231

Biological Sciences - Article

Keywords:

Posted Date: September 9th, 2021

DOI: https://doi.org/10.21203/rs.3.rs-842556/v1

Additional Declarations: There is **NO** Competing Interest.

Title: Bacterial infection drives trained immunity through epigenetic remodeling of epithelial stem cells

Authors: Seongmi K. Russell[1], Hyung Joo Lee[2,3], Benjamin Olson[1], Jonathan Livny[4], Valerie P. O'Brien[1,5], Lu Yu[1], Elisha D.O. Roberson[2,6], Shady Estfanous[7,8], Amal O. Amer[7], Marco Colonna[9], Thaddeus Stappenbeck[10], Ting Wang[2,3]*, Thomas J. Hannan[1,9]*, Scott J. Hultgren[1]*

Affiliations:

[1]Department of Molecular Microbiology and Center for Women's Infectious Disease Research, Washington University School of Medicine, St Louis, MO, USA.

[2]Department of Genetics, Washington University School of Medicine, St Louis, MO, USA.

[3]Edison Family Center for Genome Sciences and Systems Biology, Washington University School of Medicine, St Louis, MO, USA.

[4]Infectious Disease and Microbiome Program, The Broad Institute of Massachusetts Institute of Technology and Harvard, Cambridge, MA, USA.

[5]Fred Hutchinson Cancer Research Center, Human Biology Division, Seattle, WA, USA.

[6]Department of Medicine, Division of Rheumatology, Washington University School of Medicine, St Louis, MO, USA.

[7]Department of Microbial Infection and Immunity, Infectious Diseases Institute, Ohio State University, Columbus, OH, USA.

[8]Biochemistry and Molecular Biology Department, Faculty of Pharmacy, Helwan University, Cairo, Egypt.

[9]Department of Pathology and Immunology, Washington University School of Medicine, St Louis, MO, USA.

[10]Department of Inflammation and Immunity, Lerner Research Institute, Cleveland Clinic, Cleveland, OH, United States.

*Corresponding authors. Email: twang@wustl.edu (TW), thannan@wustl.edu (TJH), hultgren@wusm.wustl.edu (SJH).

ABSTRACT

Recurrent bacterial infections are a major health burden worldwide, yet the mechanisms dictating host susceptibility to recurrence are poorly understood. Here we demonstrate that an initial bacterial infection of the urinary bladder with uropathogenic *E. coli* (UPEC) can induce sustained epigenetic changes in the bladder epithelial (urothelial) stem cells that reprogram the differentiated urothelium. We established urothelial stem cell (USC) lines from isogenic mice with different urinary tract infection histories (naïve, chronic or self-resolving). Differentiation of the USC lines *in* Transwell culture resulted in polarized urothelial cultures that recapitulated distinct remodeling morphologies seen *in vivo.* In addition, we discovered differences in chromatin accessibility that segregated by disease history, resulting in differences in gene expression upon differentiation of the USC lines *in vitro,* based on ATAC-seq analysis of the USC lines. Differential basal expression of Caspase-1 led to divergent susceptibilities to inflammatory cell death upon UPEC infection. In mice with a history of chronic infection, enhanced caspase 1-mediated inflammatory cell death was found to be a protective response that enhanced bacterial clearance upon challenge infection. Thus, UPEC infection reshapes the epigenome leading to epithelial-intrinsic remodeling that trains the mucosal immune response to subsequent infection. These findings may have broad implications for the prevention of chronic/recurrent bacterial infections.

INTRODUCTION

Recurrent infections are a major problem worldwide but little or nothing is known regarding how history of infection can increase susceptibility to another infection as can be the case for urinary tract infections (UTIs), which are one of the most common bacterial infections worldwide and are a significant cause of morbidity in otherwise healthy females[1,2]. The high recurrence rate in susceptible individuals makes treatment challenging[3]. One of the strongest risk factors for recurrent UTI (rUTI) is a history of prior UTIs[2], but the biological basis for this phenomenon is poorly understood.

In the absence of effective antibiotic therapy, acute UTIs in humans either self-resolve or develop into long-lasting chronic infections[4]. Infection of C3H/HeN mice with uropathogenic *Escherichia coli* (UPEC) recapitulates these two outcomes, i.e. self-resolving or chronic infection. Experimentally, chronic cystitis in these mice is defined as persistent high titer bacteriuria (bacteria in urine) accompanied by chronic inflammation[5,6]. Analysis of bladders with these two disease histories, after antibiotic therapy and a 4 week convalescent period, reveals that infection leads to differential bladder remodeling depending on disease history. Infection of mice having a history of self-resolution of the initial UTI (herein termed Resolved mice) results in an accelerated bladder TNFα/cyclooxygenase-2 (Cox-2) response that quickly wanes. This dynamic response promotes the rapid elimination of infection and promotes mucosal healing and hence Resolved mice are resistant to rUTIs[7,8]. In contrast, mice with a history of chronic cystitis (herein termed Sensitized mice)[7,8] are highly susceptible to rUTIs upon challenge, in part due to a robust and sustained expression of TNFα/Cox-2 in the bladder that does not wane, resulting in unchecked neutrophil transmigration across the bladder epithelium (urothelium) and mucosal wounding that promotes severe recurrent bacterial infections[6,9]. Sensitized bladders are also distinguished by histologically

apparent remodeling of the mucosa, including urothelial hyperplasia, reduced terminal differentiation of the luminal facing superficial facet cells, and lymphonodular hyperplasia. Thus, depending on disease history, the bladder tissue is differentially remodeled in a way that either increases or decreases susceptibility to rUTI.

This led to our hypothesis that bladder mucosal remodeling is mediated, in part, by epigenetic changes in urothelial stem cells (USCs) that impact bladder mucosal defense against subsequent infections[6,10]. To test this, we isolated epithelial cells from the bladders of mice with different disease histories, established primary USC lines, and propagated them in cell culture for many generations (40 or more passages). We found that USCs formed polarized and fully differentiated *in vitro* urothelium, referred to herein as **differentiated urothelium (or urothelia),** when cultured on Transwells. Importantly, we found that differentiated urothelia originating from Sensitized or Resolved mice displayed morphological phenotypes that resembled the urothelial remodeling phenotypes observed *in vivo*, relative to Naïve (never-infected) mice[10]. Using Assay for Transposase-Accessible Chromatin using sequencing (ATAC-seq)[11], we identified differences in chromatin accessibility in the USCs as a consequence of disease history, which in many cases corresponded with differences in transcriptional responses, particularly in programmed cell death pathways. These studies are the first to demonstrate epigenetic evidence of mucosal epithelial-intrinsic memory of a prior infection. This trained immunity, i.e, antigen non-specific tissue adaptations to inflammation[12], alters the bladder innate mucosal response to subsequent infections, depending on the original disease outcome. This finding may explain the prevalence of rUTI and have important therapeutic implications and chronic/recurrent bacterial infections in general.

Differentiated urothelium originating from juvenile C3H/HeN mice recapitulates mouse urothelium *in vitro*

To study urothelial-intrinsic changes that result from a prior infection, we adapted a method for the *in vitro* propagation of primary intestinal epithelial stem cells in three-dimensional (3D) culture[13,14] for use in culturing urothelial stem cells (USCs). To validate this approach, we first isolated primary urothelial cells from 8 week old Naïve C3H/HeN mice and cultured them suspended in matrigel with 50% L-WRN conditioned media (CM) (Fig. 1a, Extended Data Fig. 1a). In order to evaluate the pluripotency and Wnt signaling activation state of the USCs in this culture system, we measured the expression of *Trp63*, which encodes the stem cell marker transformation-related protein 63 (p63), and *Axin2*, a Wnt-target gene[14], by RT-qPCR (Extended Data Fig. 1b-d). *Trp63* and *Axin2* gene expression remained high through the first 3 days of culture in 50% CM, then decreased by 5 to 7 days. Switching to 5% CM after 3 days also reduced expression of *Axin2* at 5 days, showing that extended culture or lower CM percentage can reduce Wnt signaling. Expression of uroplakin-3a (*Upk3a*), a surface protein expressed by differentiated urothelial cells, was significantly increased in 5% CM compared with 50% CM at 7 days (Extended Data Fig. 1d), indicating that the USCs had begun to differentiate. After propagation of USCs in 50% CM over several passages, culturing in 0% CM in 3D culture for 5 days resulted in the development of epithelial polarity with the formation of a central cavity (Extended Data Fig. 1e). Within the resulting cysts, cavity-facing cells differentiated into superficial facet-like cells with the expression of *Upk3a*. In contrast, perimeter cells in contact with the matrigel matrix were positive for the basal urothelial cell marker cytokeratin (CK) 5.

We next established a Transwell culture system to differentiate USCs of juvenile C3H/HeN mice into polarized, stratified urothelial barriers. Human bladder carcinoma cells (ATCC HTB-9

116 [5637]), which have widely been used for the *in vitro* study of UPEC interactions with bladder
117 cells, were also cultured in Transwells to compare differences between primary USCs and cancer
118 cell lines. Primary USCs were seeded and cultured on the Transwell for 2-3 weeks (Fig. 1a), and
119 formation of intact urothelium was confirmed by robust transepithelial electrical resistance (TER)
120 (Fig. 1b). In contrast, 5637 cells did not increase TER during 2 weeks of culture in the same
121 differentiation conditions (Extended Data Fig. 2a). The examination of the differentiated urothelia
122 by confocal microscopy demonstrated that the apical surface was lined by large hexagonal
123 superficial facet cells that were positive for the terminal differentiation marker CK20 (Fig. 1c),
124 while 5637 cell cultures showed small round cells. (Extended Data Fig. 2b-c). The surface of
125 differentiated urothelia was characterized by the presence of cell junctions and uroplakin plaques
126 (Fig. 1d), similar to how superficial facet cells appear on the surface of intact bladder tissues[6],
127 along with the surface localization of terminal differentiation markers UPK3 and CK20. The stem
128 cell marker TRP63 was expressed in the basal cells, with the epithelial cell junction marker E-
129 cadherin (ECAD) expressed on the basolateral surface of all cells observed, confirming that there
130 was no contamination of other cell types such as immune cells (Fig. 1e). In contrast, although 5637
131 cells could form layers of four to six cells on Transwells, the cells were loosely connected to each
132 other and lacked evidence of polarization or junction formation when stained with differentiation
133 markers (Extended Data Fig. 2d). Altogether, the distribution of these differentiation
134 characteristics in basal and superficial urothelial layers is consistent with what is observed in
135 mouse and human bladder tissue and indicates that differentiated urothelium on the Transwell
136 provides significant advantages over a tumor cell line for studying the biology of urothelium.

137 **Differentiated urothelia originating from previously infected mice maintain bladder**
138 **remodeling phenotypes**

Using our murine model of rUTI[5,6], we have shown that an initial UTI event results in bladder remodeling, including structural and proteomic changes to the urothelium, the nature of which depends on the outcome of the initial infection, i.e., whether chronic or self-resolving. Based on the long-term characteristics of bladder remodeling, which lasts more than six months in mice[10], we hypothesized that changes in the bladder USCs play a key role in bladder remodeling. To investigate this, we isolated bladder USCs from convalescent mice (four weeks after the initiation of antibiotics), both those that self-resolved infection (Resolved), and those that had developed chronic infection (Sensitized) (Fig. 2a-b). We also isolated USCs from age-matched Naïve mice as controls (Naïve) and established different USC lines from four mice for each of the different infection histories. Following the procedures outlined above for juvenile C3H/HeN USCs, we propagated these cell lines 15-30 passages and then differentiated them on Transwells and characterized each cell line by microscopy after 2-3 weeks of culture. We found that the urothelium derived from Sensitized USCs recapitulates many of the morphological differences observed previously *in vivo*[6] even after many passages, including smaller surface cells and decreased expression of the terminal differentiation markers UPK3 and CK20 when compared with differentiated urothelium derived from Naïve USCs (Fig. 2c-e). Automated measurement of surface cell sizes showed that the apical cells of the Sensitized differentiated urothelia are significantly smaller than those in Naïve differentiated urothelia, whereas the Resolved urothelia have an intermediate phenotype, consistent with *in vivo* data (Fig. 2f-g)[6]. Collectively, these data indicate that morphological differences in the urothelium associated with bladder epithelial remodeling in previously infected mice can be recapitulated in differentiated urothelia derived from the USCs isolated from mice with corresponding infection histories.

USCs from previously infected mice have differential chromatin accessibility near inflammatory response genes

Our data showed that a prior infection results in USC-intrinsic changes and that these changes are heritable over many generations of cell culture. Therefore, we hypothesized that epigenetic changes occur in USCs as a consequence of an initial UPEC infection. To investigate the presence of differential epigenetic modification in these USCs, we assayed for genome-wide differences in chromatin accessibility via Omni-ATAC-seq, a technique for mapping regions of nuclear chromatin that are accessible to transposases by sequencing[11,15]. We identified a total of 59,801, 63,195, and 82,030 highly reproducible accessible chromatin regions in two biological replicates each of the Naïve, Resolved, and Sensitized USC lines, respectively. Principal component analysis (PCA) of these USC lines separates Sensitized USCs from other groups (Fig. 3a). Using DiffBind[16], we identified 2880 differentially accessible regions (DARs) of chromatin between Sensitized and Resolved USCs (FDR <0.05) (Fig. 3b, Supplementary Table 1). Among those 2880 regions, 925 regions are Sensitized-accessible DARs (more accessible chromatin regions in Sensitized than Resolved) and 1955 regions are Resolved-accessible DARs (more accessible chromatin regions in Resolved than Sensitized) (Fig. 3c-d).

To investigate whether the genes near these DARs were enriched for any functional annotation, we performed Gene Ontology (GO) pathway analysis on these DARs using GREAT[17]. This analysis revealed that genes associated with Sensitized-accessible DARs are strongly enriched for many biological processes involving cell death, oxidative stress, and immune response. In contrast, Resolved-accessible DARs are enriched for proliferation and differentiation related pathways (Fig. 3e-f). These enriched pathways were also previously found to be enriched

in the differentially expressed genes in whole bladder RNA-seq comparing Sensitized and Resolved mice[6], suggesting that chromatin remodeling in bladder USCs is a key determinant of bladder tissue remodeling due to chronic cystitis. We also performed RNA-seq of Naïve, Resolved, and Sensitized USCs to compare with their epigenome. Similar to the ATAC-seq analysis, PCA analysis of the RNA-seq data separates Sensitized USCs from other groups along PC1, indicating that the transcriptional profiles of Sensitized USCs are different from those of Resolved or Naïve USCs (Fig. 3g). Sensitized USCs had 108 and 73 differentially expressed genes (DEGs) compared to Naïve and Resolved USCs, respectively (Extended Data Fig. 3a-b), of which 40 genes were common to both comparisons (Fig. 3h). The top 15 DEGs included the glutathione transferase genes *Mgst1* and *Mgst3* (Fig. 3h). In contrast, no DEGs were detected between Resolved and Naïve USCs. Both the epigenomic and transcriptomic analysis of USCs suggest that Sensitized mice have heritable changes to their USCs that are evident when grown under stem cell culture conditions.

USC lines from mice with different disease histories express different differentiation programs

We next assessed the differential gene expression in differentiated urothelia. USCs were differentiated on Transwells for 2-3 weeks *in vitro* as described above and then infected with a prototypical UPEC strain, UTI89, or mock-infected with PBS for 2 hours at which time RNA was harvested for RNA-seq and transcript analyses. PCA of all DEGs showed that the transcriptional profiles of mock-infected differentiated urothelia were clustered by the infection history of USCs (Fig. 4a), indicating intrinsic differences in the differentiated urothelia due to prior infection history, in line with what was observed in USCs (Fig. 3g). Differentially expressed genes between mock-infected Sensitized and Resolved differentiated urothelia were visualized in a volcano plot

(Fig. 4b). Infection largely caused a uniform shift in the PCA plot for each cell line (Fig. 4a), likely reflecting a conserved transcriptional response to UPEC infection in each convalescent state (Extended Data Fig. 4a). To further investigate transcriptional differences between cell lines, we performed Ingenuity Pathway Analysis (IPA) using DEGs comparing mock-infected Sensitized and Resolved differentiated urothelia (Fig. 4c). Sensitized and Resolved differentiated urothelia displayed differential gene expression in pathways related to apoptosis, reactive oxygen species (ROS) response, and immune response independent of UPEC infection (Fig. 4c, Extended Data Fig. 4b-c).

Based on our *in vivo* observations that the remodeled Sensitized urothelium is characterized by severe exfoliation and Cox-2 inflammation-dependent mucosal wounding during UPEC infection[6], we specifically interrogated pathways that are related to the inflammatory cell death. **A** heatmap of gene expression shows that genes associated with programmed cell death pathways are more enriched in Sensitized differentiated urothelia compared to Resolved differentiated urothelia (Fig. 4d, Supplementary Table 2), while *Casp1* is the most significantly differentially regulated gene between Sensitized and Resolved differentiated urothelia according to IPA (Extended Data Table 1). Some pyroptosis-related genes, including *Aim2*, *Casp1*, and *Gsdmc2/3*, were upregulated in Sensitized differentiated urothelia while other pyroptosis-related genes, as well as apoptosis and necroptosis-related genes were upregulated in Resolved differentiated urothelia compared to Naïve and Sensitized differentiated urothelia, suggesting that Resolved and Sensitized cells have different programmed cell death mechanisms during UPEC infection. Consistent with our previous *in vivo* studies which showed bladder remodeling after a prior infection, these data indicate the presence of an epithelial-intrinsic memory of infection.

Sensitized differentiated urothelia are reprogrammed to express increased levels of Caspase 1, revealing a mechanism of epithelial-intrinsic trained immunity

RNA-seq fold-changes did not generally correspond well with local ATAC-seq fold-changes (Extended Data Fig. 5a-b). This may be in part because accessible chromatin regions distal to the associated genes may or may not be acting to regulate the transcription of those genes and that differentiation is likely to change chromatin structure and accessibility. However, we reasoned that increased chromatin accessibility directly at gene promoter regions will provide better access to TF binding sites that facilitate gene transcriptional regulation. To focus on changes at the promoter sites, we selected DAR-neighboring genes whose promoter sites are located within 5 kb of DARs, then collected overlapping genes from Sensitized-enriched or Resolved-enriched DEGs (Fig. 5a). We found that inflammatory response related genes including *Casp1* and *Gdf15* showed highly positive correlations between chromatin accessibility proximal to their promoters and gene expression, which suggested that these inflammatory sensor genes are primed upon initial chronic infection and may allow a faster response to secondary infection (Fig. 5a-b).

In mouse and human, both Caspase 1 and Caspase 4 (in the mouse, the *Casp4* gene encodes Caspase 11) have been shown to be involved in pyroptotic cell death, although Caspase function may vary depending on cell or stimulus type[18,19]. Here we found that *Casp1* and pyroptosis related genes were more highly expressed in Sensitized differentiated urothelia (Fig. 4f), and chromatin accessibility of the *Casp1* promoter region was also highly increased in Sensitized USCs compared to Resolved USCs (Fig. 5a-b). To validate differential gene expression of *Casp1*, we performed RT-qPCR using differentiated urothelia. As we observed in the RNA-seq of differentiated urothelia, *Casp1* was more highly expressed in Sensitized differentiated urothelia compared to Resolved, independent of UPEC infection (Fig. 5c). In contrast, *Casp4* genes were similarly

induced by UPEC infection in all cell lines (Fig. 5c). Concordantly, immunoblot staining showed that only Sensitized differentiated urothelia expressed Caspase 1 (Fig. 5d), in agreement with our previous *ex vivo* proteomics of convalescent Sensitized mouse bladders[9], which demonstrated that Caspase 1 is enriched in Sensitized relative to Resolved urothelium.

In our previous studies, we found that the secreted pore-forming bacterial toxin α-hemolysin (HlyA), commonly produced by UPEC, induces Caspase 1/11-dependent inflammasome-mediated cell death in human and mouse urothelial cells[18]. *HlyA* expression is normally tightly regulated by the CpxRA two-component system, but *hlyA* overexpression in a *cpxR* deletion mutant induces robust urothelial exfoliation and reduced bacterial burdens. Inhibition of Caspase 1/11 restored virulence of the *HlyA* overexpressing UPEC strain, demonstrating that Caspase 1-mediated pyroptotic cell death is protective against UPEC infection[18]. However, while protective in naive mice, pyroptotic exfoliation could act as a double-edged sword in Sensitized mice, exacerbating the COX-2 dependent inflammation and mucosal wounding that allows severe acute rUTI[9]. Based on this evidence, we hypothesized that enhanced Caspase 1 expression in the Sensitized differentiated urothelium leads to a more robust pyroptotic cell death response upon wild type (HlyA+) UPEC infection *in vitro*. An LDH cytotoxicity assay demonstrated that UPEC infection induced cell death in Naïve, Resolved, and Sensitized differentiated urothelia (Fig. 5e), but cell death was significantly greater in Sensitized differentiated urothelia. We next performed challenge infections using WT UTI89 and UTI89Δ*hlyA* strains in Naïve, Resolved and Sensitized mice. Sensitized mice have lower bacterial burdens upon WT UTI89 infection compared to Resolved and Naïve mice at 6 hpi (Fig. 5f). We observed that Δ*hlyA* infection, which doesn't activate Caspase 1-mediated pyroptotic cell death, showed significantly increased bacterial burdens in Sensitized mice compared to WT, whereas

there were no differences in Naïve and Resolved mice (Fig. 5f). This indicates that Sensitized mice are protected by Caspase 1-mediated pyroptotic cell death during early UPEC infection. We also extended the length of the secondary challenge infection to 28 days to investigate phenotypic differences in disease outcome. The incidence of recurrent chronic cystitis at 28 dpi was significantly increased in Sensitized mice when infected with Δ*hlyA* compared to WT. Naïve mice are generally less susceptible to chronic cystitis as they age and there was no difference in the overall low incidence of chronic cystitis between Δ*hlyA* and WT strains (Fig. 5g). Resolved mice did not develop recurrent chronic cystitis with either bacterial strain, in accordance with their previously established resistance to rUTI. These findings indicate that Caspase 1 overexpression in Sensitized urothelial cells is a protective response that helps to resolve challenge UPEC infection during early UTI, revealing an epithelial-intrinsic mechanism of trained immunity, although this protective response is often outcompeted by Cox-2 mediated inflammation leading to rUTI.

DISCUSSION

Previous studies have shown that bladder tissue remodeling occurs in response to UPEC infection and this remodeling is accompanied by changes in susceptibility to subsequent infection, depending on prior infection outcomes[5-7]. We hypothesized that this altered susceptibility was mediated, at least in part, by the development of trained immunity at the bladder mucosa. In contrast with adaptive immunity, which encompasses antigen-specific responses by T and B lymphocytes, “trained immunity” is characterized by antigen non-specific tissue adaptation to acute and chronic inflammation, sometimes in response to infection, and has been predominantly studied in professional immune cells, such as macrophages, monocytes, dendritic cells, and natural

296 killer cells[20-22]. However, the long-lasting bladder remodeling phenotypes and other morphological,
297 transcriptional, and functional changes seen in mice previously infected with UPEC suggested the
298 possibility that epithelial stem cells were being reprogrammed as a mechanism of trained immunity.

299 Here we used a primary epithelial cell culture system[14] to study the urothelial-intrinsic
300 contribution to bladder mucosal remodeling. Strikingly, we found that urothelial remodeling
301 changes observed in previously infected mice could be recapitulated *in vitro* by differentiating the
302 respective USC lines. Furthermore, we detected differences in USC chromatin accessibility that
303 segregate by disease history, thus providing an epigenetic mechanism of these long-lasting
304 phenotypes. Lastly, while the undifferentiated USCs displayed few examples of differential gene
305 expression between the different disease histories, we observed broad differential gene expression
306 upon differentiation in Transwell culture, particularly with regard to urothelial cell death. The
307 mechanism of differential gene expression in differentiated urothelia originating from the different
308 USC lines likely involves differentiation-induced TF binding within these differentially accessible
309 regions.

310 The bladder urothelium of previously infected mice is known to be resistant to intracellular
311 colonization relative to age-matched Naïve mice[6,7]. However, the mechanisms for this intracellular
312 colonization resistance differs between Resolved and Sensitized mice. In Resolved mice, UPEC
313 initially form intracellular bacterial communities (IBCs) in the urothelial cells, similar to Adult
314 Naïve mice, but they are rapidly shed within the first 6 hours of infection via enhanced TNFα-
315 mediated inflammation[7]. In contrast, IBCs do not form at all in Sensitized urothelium *in vivo*, likely
316 due to the small cell size and actin-gating of the incompletely differentiated superficial cells[6,23]. In
317 this work, we have further illuminated this protective response by elucidating how the Resolved

318 and Sensitized urothelia are differentially reprogrammed with regard to the basal levels of
319 expression of cell death machinery components. Our data suggest that HlyA-mediated cell death,
320 which results in urothelial exfoliation, plays a protective role in reducing early bladder
321 colonization in Sensitized bladders. This effect is likely a consequence of the increased baseline
322 expression of Caspase 1 and perhaps other inflammasome-associated factors, such as Gasdermins
323 C2 and C3 that can act as terminal effectors of inflammatory cell lysis[24], effects observed here *in*
324 *vitro* and previously described in *ex vivo* proteomics studies of mouse urothelia[9]. Expression of
325 *Aim2*, which encodes a cytosolic innate immune sensor that can activate the Caspase 1
326 inflammasome, was also more highly expressed in Sensitized differentiated urothelia. In the skin
327 of mice, epigenetic modification of the *Aim2* locus after a primary inflammation induced by
328 imiquimod and resulting inflammation enables the skin to have a more rapid response to a
329 secondary inflammatory insult[25], suggesting that epigenetic reprogramming of inflammasome
330 components may be a common mechanism for priming inflammation sensors to prepare for
331 secondary exposure at barrier tissue sites.

332 Thus, we have delineated mechanisms of epithelial-intrinsic trained immunity in Sensitized
333 mice that are protective against rUTIs[5-7]. However, it is important to note that Sensitized mice have
334 competing protective and sensitizing responses to challenge infection, which typically manifests
335 as an extreme bimodal distribution of infection burdens by 24 hpi[5]. As such, this protective trained
336 immunity in Sensitized urothelium is nevertheless often overcome by Cox-2 inflammation-
337 dependent mucosal wounding that occurs later during the first 24 hours of acute rUTI at the basal
338 urothelial cell level, thereby transforming the colonization landscape in favor of the bacteria[6,9].
339 The activities of Cox-2 and downstream eicosanoid synthetic machinery and effectors are closely
340 linked to the level of oxidative stress within the cell[26]. Interestingly, we found that Sensitized

differentiated urothelia displayed increased expression of factors associated with glutathione-mediated detoxification pathways relative to Resolved differentiated urothelia (Fig. 4c). However, RNA-seq of Sensitized USCs demonstrated reduced expression of these same factors, particularly of enzymes that detoxify oxidative radicals such as microsomal glutathione S-transferase 1 (Fig. 3h, Extended Data Fig 3c-d), which resembles *ex vivo* proteomics of the Sensitized urothelium[9]. Decreased levels of these protective enzymes, particularly at the stem cell level of the urothelium where *Cox-2* expression is greatest during UPEC infection[9], could explain why Sensitized urothelia are so prone to severe mucosal wounding during UPEC infection *in vivo*, leading to overwhelming bacterial colonization.

Here, we elucidate that a common bacterial infection can induce epigenetic changes in stem cells. Further, this epigenetic imprint leads to an epithelial-intrinsic remodeling that trains the mucosal immune response to subsequent infection. Thus, pathogenic bacteria and the host inflammatory responses that they elicit can be considered as potential epimutagens able to reshape the epigenome. Our discovery of epithelial stem cell epigenetic reprogramming upon UPEC infection has implications for understanding the mechanism of epithelial-intrinsic trained immunity against other types of infection or inflammatory disease. Further mechanistic studies of chromatin remodeling in epithelial stem cells may lead to novel therapies for a range of recurrent infections and inflammatory conditions in various diseases. For example, therapeutic use of an inhibitor of histone demethylase LSD1, which is overexpressed in skin epithelial cancer, drives significant increases in H3K4 methylation in the cells thus leading to both premature epidermal differentiation and the repression of squamous cell carcinoma[27]. Therefore, investigation into DNA methylation, acetylation, and histone modification responses to infection and how this differs with

363 UPEC infection outcome could shed light on potential therapeutic targets to prevent rUTIs and/or
364 reverse the epigenetic priming that leads to increased susceptibility to recurrent disease.

365

366 **Main References**

367 1 Foxman, B. Epidemiology of urinary tract infections: incidence, morbidity, and economic
368 costs. *Dis Mon* **49**, 53-70, doi:10.1067/mda.2003.7 (2003).
369 2 Foxman, B., Barlow, R., D'Arcy, H., Gillespie, B. & Sobel, J. D. Urinary tract infection:
370 self-reported incidence and associated costs. *Ann Epidemiol* **10**, 509-515 (2000).
371 3 Godaly, G., Ambite, I. & Svanborg, C. Innate immunity and genetic determinants of
372 urinary tract infection susceptibility. *Curr Opin Infect Dis* **28**, 88-96,
373 doi:10.1097/QCO.0000000000000127 (2015).
374 4 Foxman, B. The epidemiology of urinary tract infection. *Nat Rev Urol* **7**, 653-660,
375 doi:10.1038/nrurol.2010.190 (2010).
376 5 Hannan, T. J., Mysorekar, I. U., Hung, C. S., Isaacson-Schmid, M. L. & Hultgren, S. J.
377 Early severe inflammatory responses to uropathogenic E. coli predispose to chronic and
378 recurrent urinary tract infection. *PLoS Pathog* **6**, e1001042,
379 doi:10.1371/journal.ppat.1001042 (2010).
380 6 O'Brien, V. P. *et al.* A mucosal imprint left by prior Escherichia coli bladder infection
381 sensitizes to recurrent disease. *Nat Microbiol* **2**, 16196, doi:10.1038/nmicrobiol.2016.196
382 (2016).
383 7 Yu, L. *et al.* Mucosal infection rewires TNFa signaling dynamics to skew susceptibility
384 to recurrence. *Elife* **8**, doi:10.7554/eLife.46677 (2019).

8 Anderson, G. G. *et al.* Intracellular bacterial biofilm-like pods in urinary tract infections. *Science* **301**, 105-107, doi:10.1126/science.1084550 (2003).

9 Hannan, T. J. *et al.* Inhibition of Cyclooxygenase-2 Prevents Chronic and Recurrent Cystitis. *EBioMedicine* **1**, 46-57, doi:10.1016/j.ebiom.2014.10.011 (2014).

10 O'Brien, V. P., Dorsey, D. A., Hannan, T. J. & Hultgren, S. J. Host restriction of Escherichia coli recurrent urinary tract infection occurs in a bacterial strain-specific manner. *PLoS Pathog* **14**, e1007457, doi:10.1371/journal.ppat.1007457 (2018).

11 Buenrostro, J. D., Giresi, P. G., Zaba, L. C., Chang, H. Y. & Greenleaf, W. J. Transposition of native chromatin for fast and sensitive epigenomic profiling of open chromatin, DNA-binding proteins and nucleosome position. *Nat Methods* **10**, 1213-1218, doi:10.1038/nmeth.2688 (2013).

12 Netea, M. G. *et al.* Defining trained immunity and its role in health and disease. *Nat Rev Immunol* **20**, 375-388, doi:10.1038/s41577-020-0285-6 (2020).

13 Miyoshi, H. & Stappenbeck, T. S. In vitro expansion and genetic modification of gastrointestinal stem cells in spheroid culture. *Nat Protoc* **8**, 2471-2482, doi:10.1038/nprot.2013.153 (2013).

14 VanDussen, K. L. *et al.* Development of an enhanced human gastrointestinal epithelial culture system to facilitate patient-based assays. *Gut* **64**, 911-920, doi:10.1136/gutjnl-2013-306651 (2015).

15 Corces, M. R. *et al.* An improved ATAC-seq protocol reduces background and enables interrogation of frozen tissues. *Nat Methods* **14**, 959-962, doi:10.1038/nmeth.4396 (2017).

16 Ross-Innes, C. S. *et al.* Differential oestrogen receptor binding is associated with clinical outcome in breast cancer. *Nature* **481**, 389-393, doi:10.1038/nature10730 (2012).

17 McLean, C. Y. *et al.* GREAT improves functional interpretation of cis-regulatory regions. *Nat Biotechnol* **28**, 495-501, doi:10.1038/nbt.1630 (2010).

18 Nagamatsu, K. *et al.* Dysregulation of Escherichia coli alpha-hemolysin expression alters the course of acute and persistent urinary tract infection. *Proc Natl Acad Sci U S A* **112**, E871-880, doi:10.1073/pnas.1500374112 (2015).

19 Lee, D. J. *et al.* Regulation and Function of the Caspase-1 in an Inflammatory Microenvironment. *J Invest Dermatol* **135**, 2012-2020, doi:10.1038/jid.2015.119 (2015).

20 Saeed, S. *et al.* Epigenetic programming of monocyte-to-macrophage differentiation and trained innate immunity. *Science* **345**, 1251086, doi:10.1126/science.1251086 (2014).

21 Hole, C. R. *et al.* Induction of memory-like dendritic cell responses in vivo. *Nat Commun* **10**, 2955, doi:10.1038/s41467-019-10486-5 (2019).

22 Min-Oo, G. & Lanier, L. L. Cytomegalovirus generates long-lived antigen-specific NK cells with diminished bystander activation to heterologous infection. *J Exp Med* **211**, 2669-2680, doi:10.1084/jem.20141172 (2014).

23 Eto, D. S., Sundsbak, J. L. & Mulvey, M. A. Actin-gated intracellular growth and resurgence of uropathogenic Escherichia coli. *Cell Microbiol* **8**, 704-717, doi:10.1111/j.1462-5822.2006.00691.x (2006).

24 Hou, J. *et al.* PD-L1-mediated gasdermin C expression switches apoptosis to pyroptosis in cancer cells and facilitates tumour necrosis. *Nat Cell Biol* **22**, 1264-1275, doi:10.1038/s41556-020-0575-z (2020).

25 Naik, S. *et al.* Inflammatory memory sensitizes skin epithelial stem cells to tissue damage. *Nature* **550**, 475-480, doi:10.1038/nature24271 (2017).

26 Lu, Y. & Wahl, L. M. Oxidative stress augments the production of matrix metalloproteinase-1, cyclooxygenase-2, and prostaglandin E2 through enhancement of NF-kappa B activity in lipopolysaccharide-activated human primary monocytes. *J Immunol* **175**, 5423-5429, doi:10.4049/jimmunol.175.8.5423 (2005).

27 Egolf, S. *et al.* LSD1 Inhibition Promotes Epithelial Differentiation through Derepression of Fate-Determining Transcription Factors. *Cell Rep* **28**, 1981-1992 e1987, doi:10.1016/j.celrep.2019.07.058 (2019).

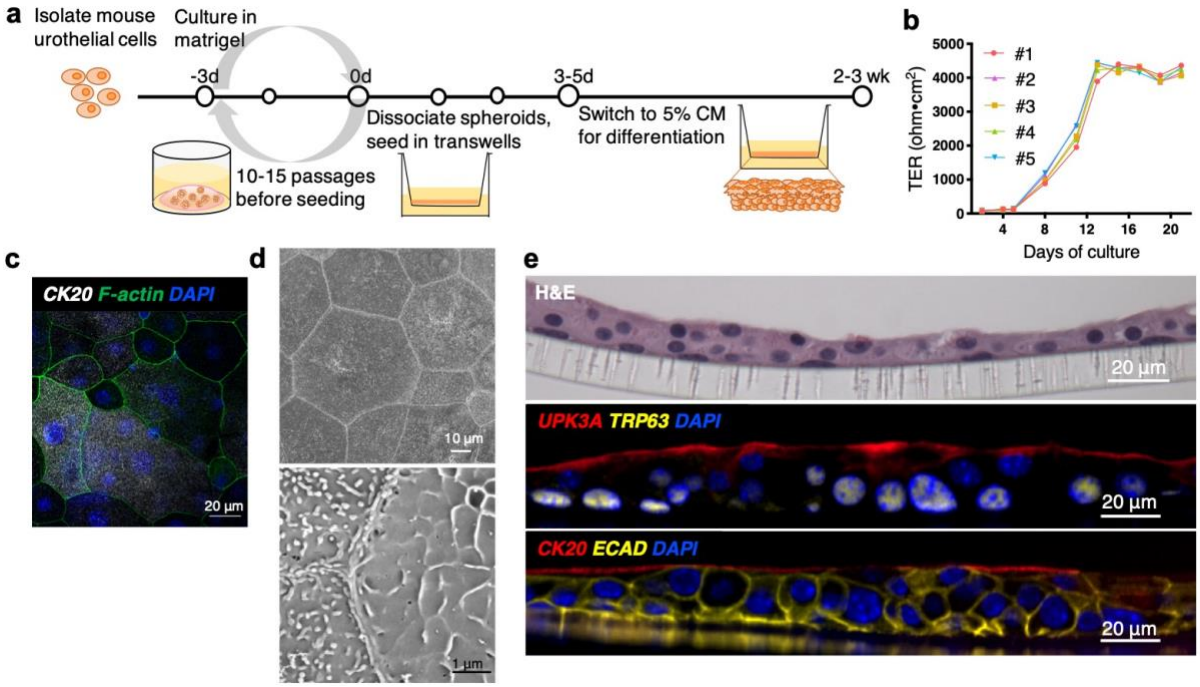

Fig. 1. The culture of urothelial stem cells (USCs) of juvenile C3H/HeN mice regenerates differentiated urothelium *in vitro*. (**A**) USCs isolated from 8 week old C3H/HeN mice are expanded by spheroidal culture in matrigel with 50% L-WRN conditioned media (CM) including Y27632, ROCK inhibitor, and SB431542, TGF β type 1 inhibitor. After 3 days of spheroid culture, cells are dissociated into a single cell suspension and 3-4x10^5 cells were seeded onto the Transwell membrane. The cells are cultured in 50% CM for 3-5 days then cultured in 5% CM for 2-3 weeks until full differentiation. (**B**) Cell cultures with a TER value >4000 ohm*cm^2 were then analyzed (5 Transwells cultured from one juvenile C3H/HeN cell line). For consistency, TER was measured 1 day after media change. (**C-D**) Differentiated urothelia on the Transwells were fixed and imaged via (**C**) confocal microscopy and (**D**) scanning electron microscopy (SEM) to show the top-down view of urothelium. In (**C**) samples were stained for F-actin, the terminal differentiation marker CK20, and nuclei (DAPI). (**E**) The urothelia were also paraffin-embedded, sectioned and immunostained for: epithelial differentiation markers UPK3A and CK20, epithelial junction

453 marker E-cadherin, stem cell marker TRP63, and nuclear marker DAPI. Representative images are
454 shown. Data come from 2-3 independent experiments using USCs from 5 different juvenile
455 C3H/HeN mice.

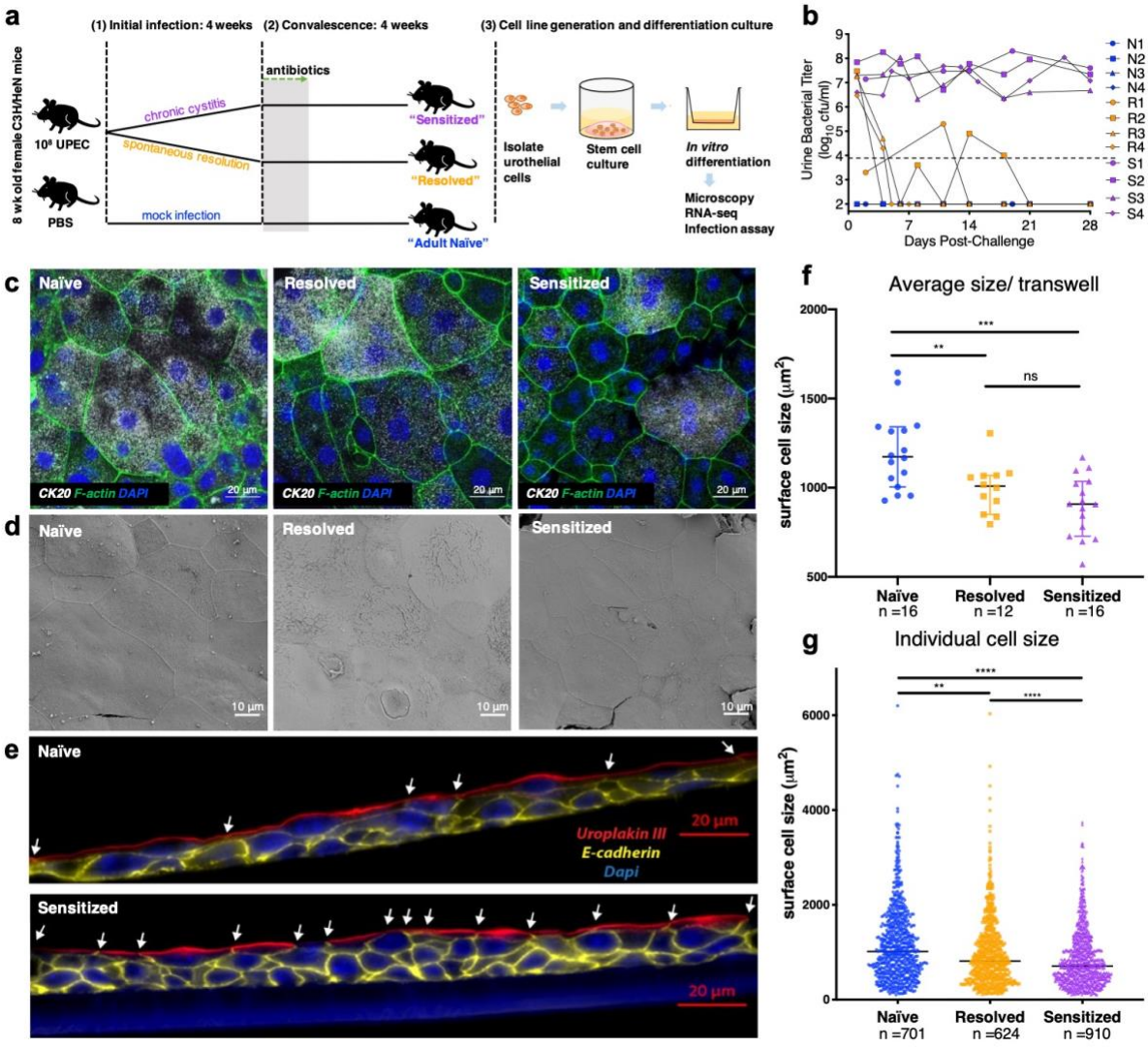

Fig. 2. Differentiated urothelia originating from previously infected mice maintain bladder remodeling phenotypes. (**A**) Time course of initial infection with 10^8 cfu UTI89 Kan^R and convalescent period in C3H/HeN mice and (**B**) representative urine bacterial titer time course over 4 wpi. Dashed horizontal line represents the cutoff for significant bacteriuria: 10^4 cfu/ml. Naïve, Resolved and Sensitized mice were named as N1-4 (blue), R1-4 (orange), and S1-4 (purple). (**C-D**) USCs isolated from these mice were cultured into differentiated urothelium on Transwells, fixed and imaged via (**C**) confocal microscopy and (**D**) SEM. In (**C**) the urothelia were stained for F-actin (Phalloidin), CK20, E-cadherin, and nuclei (DAPI). (**E**) Transwells were paraffin-

embedded, sectioned and immunostained for UPK3A, E-cadherin, and nuclei. White arrows show cell junctions indicating size of surface cells. (**F-G**) Fixed slides processed from 44 Transwells of Naïve, Resolved, and Sensitized (n=16, 12, and 16 Transwells from n=4, 3, 4 mice, respectively) were stained for CK20, E-cadherin, and nuclei, labeled and imaged in a double-blind manner. Then the superficial cell sizes were automatically measured using the Fiji ImageJ macro program and plotted for (**F**) average cell size per each Transwell and (**G**) individual cell size, represented as median with 95% CI.

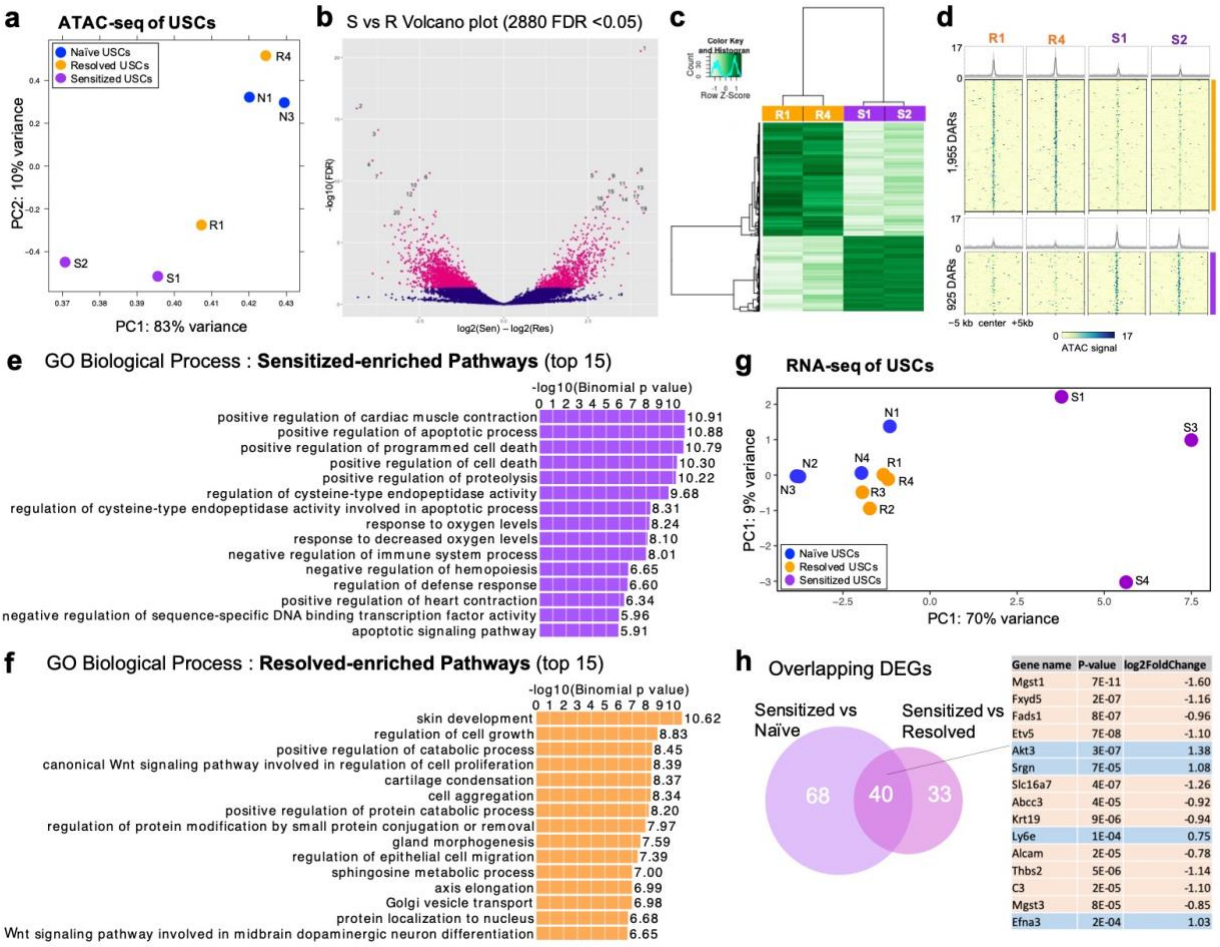

Fig. 3. Convalescent mouse USCs have differential chromatin accessibility near inflammatory response genes. Omni-ATAC-seq was performed using USCs of Naïve, Resolved, and Sensitized cells (cell lines N1, N3, R1, R4, S1, and S2, each from an individual mouse). Differentially accessible regions (DARs) across the USC cell lines are shown as (**A**) a PCA plot, and significantly differential peaks (FDR <0.05) comparing Sensitized vs. Resolved USCs are shown as (**B**) a volcano plot. The top 20 of Sensitized vs. Resolved DARs are indicated as number 1 to 20 on the graph. (**C**) Out of all 2880 DARs, 925 regions are Sensitized-accessible DARs and 1955 regions are Resolved-accessible DARs. (**D**) Average ATAC-seq signals are plotted over 10 kb regions centered on the DARs. (**E-F**) Top 15 enriched GO terms for (**E**) Sensitized (fold change

482 >1.5, FDR <0.05) and (**F**) Resolved-enriched DAR (fold change <-1.5, FDR <0.05) are analyzed
483 using GREAT. (**G**) RNA-seq was performed using USCs of Naïve, Resolved, and Sensitized cells
484 (cell lines of N1-4, R1-4, S1, and S3-4 from an individual mouse). Differentially expressed genes
485 (DEGs) across the USC cell lines are shown as a PCA plot. (**H**) The Venn diagram shows 40 DEGs
486 that overlapped between Sensitized vs Naïve and Sensitized vs Resolved, and the top 15
487 overlapping DEGs are listed.

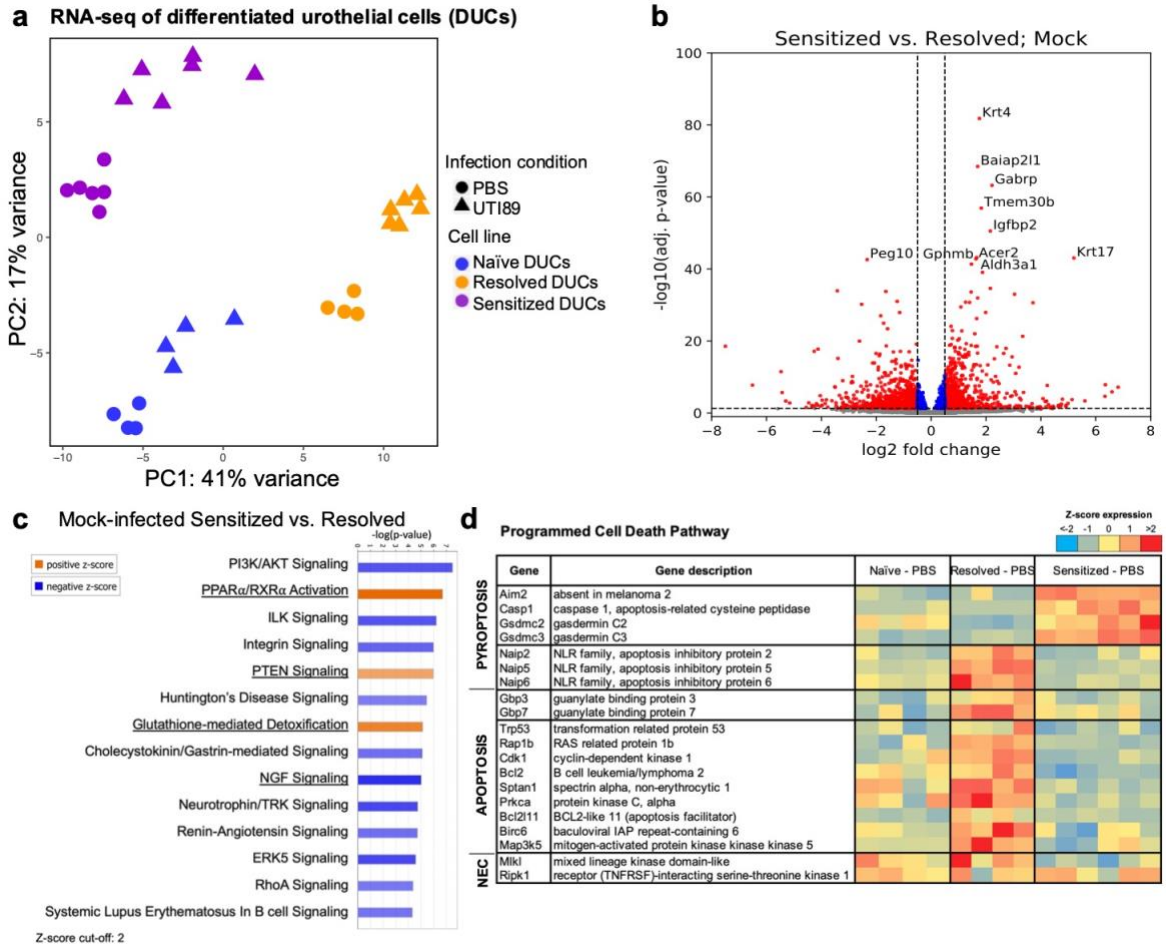

Fig. 4. Differentiated urothelia originating from convalescent mice maintain differential transcriptomics observed *in vivo*. RNA was isolated from Naïve, Resolved, and Sensitized differentiated urothelia with or without UPEC infection at 2 hpi (n=8, 10, and 12 from cell lines of N3, R3, and S3, respectively), then analyzed by RNA-seq to assess differential gene expression. (**A**) The PCA of DEGs shows clustering by cell lines (prior infection outcome) and secondary infection condition. (**B**) A volcano plot comparing mock-infected Sensitized vs. Resolved differentiated urothelial is shown. (**C**) Pathway analysis was used to assess the biological pathways enriched in differentially expressed genes in mock-infected Sensitized relative to Resolved differentiated urothelia, and significance was determined by a right-tailed Fisher's exact test, with

498 P-adjusted <0.05 considered significantly enriched pathways. Shown are selected pathways with
499 z-score > 2 and –log(p-value) > 4.2 from the specific enriched pathways by Ingenuity IPA. (**D**)
500 The heatmap shows programmed cell death associated genes which are differentially expressed in
501 mock-infected Naïve, Resolved, and Sensitized differentiated urothelia.

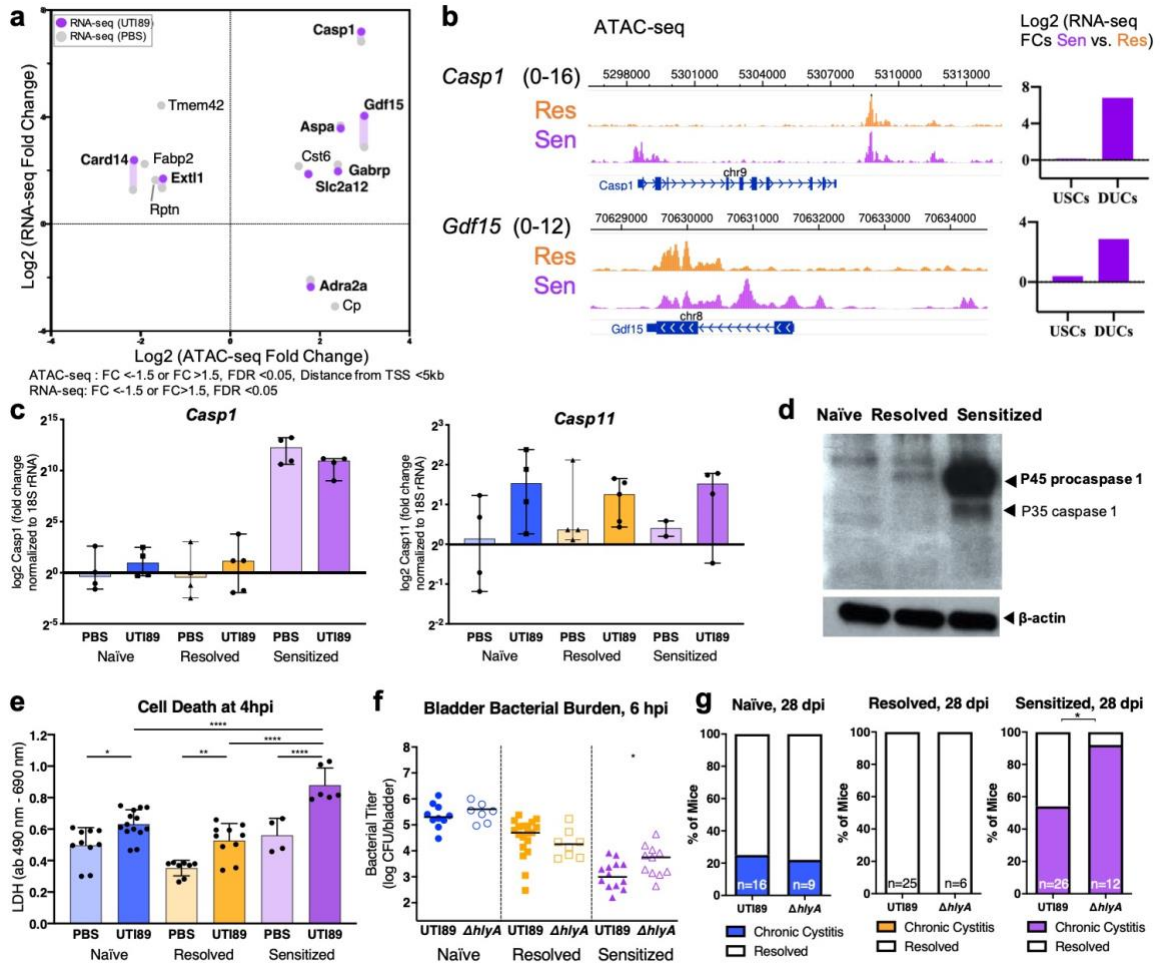

502

503 **Fig. 5. Increased Caspase 1-mediated inflammatory cell death in Sensitized USCs protects**
504 **Sensitized mice from acute and chronic UPEC infection.** (**A**) Promoter-closed genes meeting
505 indicated cut-offs were selected to find a correlation with the DEGs of Sensitized differentiated
506 urothelia with or without infection. (**B**) ATAC-seq signals of *Casp1* and *Gdf15* were visualized
507 using the WashU epigenome browser map and fold change gene expressions (USCs and
508 differentiated urothelial cells [DUCs]) of *Casp1* and *Gdf15* were plotted. (**C**) *Casp1* and *Casp4*
509 gene expression in differentiated urothelia was measured by RT-qPCR (data are represented as
510 mean ± SD) and (**D**) protein expression of Caspase 1 was assessed by western blot. (**E**) Cell death
511 of differentiated urothelia 4 hours after UTI89 infection was measured with a lactate

dehydrogenase (LDH) assay. Data are represented as mean ± SD and significance was determined with a one-way ANOVA. (**F-G**) Naïve, Resolved, and Sensitized mice were challenged with 10^7 cfu of WT UTI89 (HlyA+) or UTI89Δ*hlyA*. (**F**) Urine bacterial burden at 6 hpi and (**G**) incidence of chronic cystitis at 28 dpi are shown. Data are combined from two to three independent experiments. (**F**) Bars indicate median values and Mann–Whitney U test was used to determine significance. (**G**) Fisher's exact test was used to determine significance and the number of mice is indicated on the graph. *P < 0.05.

Methods

Ethics statement

All animal experimentation was conducted according to the National Institutes of Health guidelines for the housing and care of laboratory animals. All experiments were performed in accordance with institutional regulations after review and approval by the Animal Studies Committee at Washington University School of Medicine in St Louis, Missouri.

Mouse infections

Female C3H/HeN mice were obtained from Envigo (Indianapolis, IN). All mice were seven to eight weeks old ('juvenile') at the time of the initial infection. For the initial infection, a total 10^8 cfu of bacteria were inoculated into the bladder of C3H/HeN mice by transurethral catheterization as previously described[28]. C3H/HeN mice develop chronic cystitis in an infection does-dependent manner and this inoculum results in chronic cystitis in ~50% of mice[6]. To monitor infection outcomes, urine was collected at 1, 3, 7, 10, 14, 21, and 28 days post-infection (dpi)[5]. As we previously defined, 10^4 cfu/ml persistent bacteriuria is a specific and sensitive cutoff for detecting chronic cystitis[5]. Chronic cystitis during initial infection was defined as persistent high bacteriuria (>10^4 cfu/ml urine) at every time urine was collected, while resolution of cystitis was defined as urine bacterial titer dropping below the cutoff (10^4 cfu/ml urine) at least one time point. At four weeks post-infection, all mice were treated with trimethoprim and sulfamethoxazole in the drinking water for 10 days (54 and 270 μg/ml water, respectively)[6]. Urine samples were collected weekly after the initiation of antibiotics to confirm clearance of bacteriuria. Four weeks after the initiation of antibiotics, these convalescent mice (Naïve, Resolved, and Sensitized mice) were used to isolate primary urothelial stem cells (USCs) or used for secondary infection assay. For the

secondary infection, mice were challenged with 10^7 cfu of bacteria inoculated into the bladders as described above. To assess acute outcomes, mice were humanely euthanized 6-hour post-challenge and bacterial burdens were determined as described above.

Bacterial strains

The UPEC strain primarily used in this study was a kanamycin-resistant derivative of the human cystitis isolate UTI89[29]: UTI89 attHK022::COM-GFP (UTI89-KanR)[30]. For enumeration of intracellular bacteria by epifluorescence microscopy, we used UTI89 pANT4, which contains a plasmid that constitutively expresses eGFP. For both mouse and *in vitro* infection, UPEC strains were cultured statically in lysogeny broth (LB) at 37 °C. UTI89 inocula were prepared as previously described by spinning down the cultures at RT for 10 min at 3000 g, resuspended in 10 ml PBS, and diluted to approximately 2-3x10^9 cfu/ml (OD600 = 3.5)[5].

Host cell culture

Human BECs, designated 5637 (ATCC HTB-9) cells, were obtained from the American Type Culture Collection and maintained in RPMI 1640 supplemented with heat-inactivated 10% (vol/vol) FBS at 37 °C in the presence of 5% CO_2.

Primary USC isolation

The primary USC isolation and culture system was adapted and modified from primary intestinal epithelial cell culture method described in[13]. Bladder tissue from 8 weeks old juvenile Naïve C3H/HeN mice and convalescent mice (Naïve, Resolved, and Sensitized after initial infection and antibiotic treatment) were isolated and bisected, incubated in 1 ml of stripping

565 solution at 4 °C for overnight. The urothelial cells were scrapped off from the bladder tissue using
566 two forceps on sterilized tissue culture plate. Collected urothelial cells were then spun down at
567 4 °C at 300 g for 5 min, resuspended in 1 ml of fresh collagenase IV solution, and incubated with
568 rocking at 37 °C for 20 min. The cells were disaggregated by gentle pipetting, filtrated with 100
569 μm strainer, washed with 1 ml of washing media, then cultured in matrigel with 50% CM as
570 described in 3D spheroid cell culture. Initial culture might contain some non-stem urothelial cells,
571 so the cells were used for experiments after 10 passages.
572
573 **3D spheroid cell culture**
574 Primary bladder epithelial cells were isolated, grown, and maintained as 3D spheroid
575 cultures in Matrigel (BD Biosciences, San Jose, CA) as described in[13]. Cells were kept in 50% L-
576 WRN CM containing 10 mM Y-27632 and 10 mM SB431542 (R&D System, Minneapolis, MN).
577 Media were changed every 2 days, and cells were passaged every 3 days (1:2-3 split). Spheroids
578 at various passage numbers were cryopreserved for future use, then thawed when needed as
579 previously described[13].
580
581 **Urothelium culture on Transwell**
582 Spheroidal USCs at 3-day 3D culture were recovered from Matrigel by washing in PBS
583 with 0.5 mM EDTA, and then trypsinized in 0.05% Trypsin, 0.5 mM EDTA for 1 min at 37 °C.
584 The trypsin was then inactivated by adding washing media then spheroids were dissociated by
585 vigorous pipetting (using a double tip technique). The cells were then filtered through a 40 μm cell
586 strainer (BD Biosciences) and resuspended in 1 ml of washing media. The Transwells (3413;
587 Corning Costar, Tewksbury, MA) were coated in PBS with 1:40 Matrigel for 30 min at 37 °C.

Then the cell numbers were counted using hemocytometer under microscope. 3-4x10^4 cells in 100 µl of 50% L-WRN CM containing 10 mM Y-27632 (ROCK inhibitor) were seeded on top of the Transwell insert. An additional 600 µl of 50% CM were added to the apical compartment of the Transwells. On average, single cell suspensions from three wells of a 24-well spheroid plate were enough to seed a single Transwell.

Transepithelial electrical resistance (TER) measurements

TER was measured for cells in Transwells using an epithelial volt-ohm meter (World Precision Instruments, Sarasota, FL). Resistance of the urothelial multilayers was calculated by subtracting the resistance of the (membrane + media) from the resistance of the (membrane + media + cells). Each Transwell was measured in triplicate and the average value was taken. This value was then multiplied by the area of the Transwell membrane (0.33 cm^2) to obtain a final value in ohm*cm^2 [31].

***In vitro* UPEC infection assay**

When the Transwell is fully differentiated (TER value > 4000 ohm*cm^2), the Transwell inserts were washed in warm DMEM/F12 media for three times and infected with UPEC strains at intended MOI (1, 5, 10, 50, and 100) or other stimuli. The infected Transwells were incubated at 37 °C for 30 min, changed media containing 100 µg/ml gentamicin to clear the extracellular bacteria, and cultured for extended time. After infection, luminal and apical media were spun down at 2000 g at 4 °C for 5 min, froze at -20 °C for analysis if indicated. The Transwells were washed with sterile PBS then used for various analysis.

Whole-mount confocal staining

The cells cultured on Transwells or chamber slides were washed and fixed in PBS with 4% paraformaldehyde (PFA) for 15 min and rinsed three time with PBS. 100 µl of 0.2% Triton-X was treated for 10 min then dumped, and the cells were incubated in 100 µl of 2% BSA in for blocking for 30 min. After primary and secondary antibody staining and associated washes, the samples were stained with Alexa Fluor 555 Phalloidin (Molecular Probes binding to F-actin) and 4′,6-diamidino-2-phenylindole (DAPI). The samples were mounted in ProLong Gold Antifade Mountant (Thermo Fisher), then examined by confocal microscopy on a ZEISS LSM880 Laser Scanning Microscope with Airyscan. Fiji ImageJ and macro program were used to automatically calculate epithelial cell surface area in z-stacked confocal images.

Histopathology and immunofluorescence

USC spheroids or urothelium on the Transwells were fixed overnight in 10% formaldehyde at RT or 4 °C. After wash in PBS, the fixed samples are pre-embedded into 2% agar, cut vertically, put the Transwell side face up, embedded again in paraffin blocks, and sectioned. The slides were stained for H&E and immunostained for selected antibodies. For immunofluorescence staining, slides were deparaffinized, hydrated, blocked with 10% heat-inactivated horse serum (HIHS) and 0.3% triton X-100 in PBS, incubated with primary antibody in 1% HIHS and PBS overnight at 4 °C and secondary antibody in PBS for 30-60 min at RT[6]. The primary antibodies used were uroplakin-3 (mouse monoclonal, 10R-U103a, Fitzgerald), Trp63 (rabbit polyclonal, GTX102425, GeneTex), E-cadherin (goat polyclonal IgG, AF748, R&D Systems), cytokeratin 5 (chicken polyclonal, 905901, BioLegend) and cytokeratin 20 (mouse monoclonal, M7019, DAKO). Nuclei were stained with Hoechst (Thermo fisher). Samples were mounted in ProLong Gold Antifade,

and fluorescence was visualized on a Zeiss Axio Imager M2 Plus wide Field Fluorescence microscope. Antibodies are verified at 1DegreeBio (http://1degreebio.org/), except cytokeratin 5 and cytokeratin 20 (verified at manufacturers' websites)[6].

Scanning electron microscopy

Urothelium on the Transwell inserts were washed 3 times in PBS, fixed in EM fixative (2% paraformaldehyde, 2.5% glutaraldehyde in 1x PBS) for 1 hour on ice, and washed 3 times in PBS. Samples were then post-fixed in 1.0% osmium tetroxide, dehydrated in increasing concentrations of ethanol, then dehydrated at 31.1 °C and 1,072 p.s.i. for 16 min in a critical point dryer[6]. Samples were mounted on carbon tape-coated stubs and sputter-coated with gold/palladium under argon[6], then they were imaged on a Zeiss Crossbeam 540 FIB-SEM.

RNA isolation and RT-qPCR

Spheroids or cells on the Transwell were treated with reagents or infected with UPEC before RNA isolation. RNA was extracted using the RNAeasy Plus Mini Kit (Qiagen) and reverse-transcribed with iScript Reverse Transcription Supermix (BioRad). RT-qPCR for expression of Ptgs2, Casp1, Casp4, were performed as previously described[9,18]. 1 µl of 12.5 ng/µl cDNA was used with intron-spanning primers specific to each gene and iQ SYBR Green Supermix was used according to the manufacturer's instructions (Bio-Rad). Expression values were normalized to 18S expression levels, and the expression fold change relative to mock-infected cells or Naïve cells was determined by the cycle threshold (ΔΔCt) method[32]. Each sample was run in triplicate, and average Ct values were calculated.

RNA-seq and data analysis

Illumina cDNA libraries were generated using a modified version of the RNAtag-seq protocol[33,34]. Briefly, 1μg of total RNA was fragmented, depleted of genomic DNA, dephosphorylated, and ligated to DNA adapters carrying 5'-AN_8-3' barcodes of known sequence with a 5' phosphate and a 3' blocking group. Barcoded RNAs were pooled and depleted of rRNA using the RiboZero rRNA depletion kit (Illumina). A second adapter was added to cDNAs by template switching, cDNAs were amplified with oligos carrying Illumina P5 or P7 sequences, and the resulting cDNA libraries were sequenced to generate paired end reads.

Sequencing reads from each sample in a pool were demultiplexed based on their associated barcode sequence using custom scripts (https://github.com/broadinstitute/split_merge_pl). Barcode sequences were removed from the first read as were terminal G's from the second read that may have been added during template switching. Reads were then trimmed by cutadapt twice (cutadapt-v1.6), once by base quality and once by polyA or polyT repeats. Trimmed reads were then aligned to the Mus musculus mm10 genome using tophat2[35] (tophat2-v2.0.11, bowtie2-2.2.2). Gene counts were conducted by HTSeq[36] (HTSeq-v0.6.0, options: –format = bam –order = name –stranded = no –idattr = gene_id –mode = union) and read counts were assigned to annotated transcripts using Salmon_0.8.2[7,37]. Read normalization and differential expression were conducted with DESeq2_1.14.0[38]. rlog transformations of DESeq normalized reads were used for PCA plots. FPKM normalization of DEseq2 reads was used for z-score heatmaps. Pathway analyses were performed with Ingenuity Pathway Analysis (IPA).

ATAC-seq and data analysis

To generate chromatin accessibility profiles for Naïve, Resolved, and Sensitized USCs, Omni-ATAC libraries were generated as previously described[15]. Briefly, 2-3 wells of spheroid cultures were dissociated to prepare 1-2x10^5 cells for each sample. After nuclei preparation, 50,000 nuclei were counted and transferred into 25 µl of 2x TD buffer. 25 µl of Omni-ATAC ATAC-seq reaction mix including TDE1 enzyme was added to 25 µl of 50,000 nuclei in 2x TD buffer, then the samples were incubated at 37 °C for 30 min (tapped every 10 min during the incubation in a heat block). Transposed DNA fragments were immediately purified by using a MinElute PCR Purification Kit (Qiagen). ATAC-seq libraries were amplified by using 10-12 cycles of PCR amplification with an initial 5-min extension at 72 °C and purified by using AMPure XP Beads (Beckman Coulter). The purified libraries were eluted with 20 µl of nuclease-free water, quantified using Qubit dsDNA HS Assay Kit, and their size distribution was checked with 4200 TapeStation (High Sensitivity D1000 ScreenTape and Reagents) to ensure good RNA quality. Paired-end ATAC-seq libraries were sequenced on an Illumina NextSeq 500 machine, with a total of ~350 million reads.

ATAC-seq analysis was performed as previously described[39] and used the following tools and versions: Fastqc v0.11.5, Cutadapt v.1.11, Samtools v1.5, Bowtie2 v2.3.0, picard v2.10.0, Macs2 v2.1.1.20160309, bedtools v2.26.0. Sequencing reads were de-multiplexed by using sample-specific index sequences, quality checked with fastqc, trimmed by using cutadapt, and aligned to a reference mouse genome (mm10) by using bowtie2[40] with these parameters: --local -X 2000 --mm. Picard was then used to remove secondary alignment, multiply mapped reads, and PCR duplicated reads, and peak calling was done with MACS2[41], with these parameters: -g 1.87e9 --keep-dup all -B --SPMR --nomodel --extsize 73 --shift -37 -p 0.01 --call-summits. Irreproducible discovery rate (IDR) analysis with two replicates was performed following ENCODE's

guidelines[42], and ATAC peaks with IDR < 0.05 were chosen as highly reproducible accessible chromatin regions for further analysis. The ATAC-seq signals were visualized on the WashU Epigenome Browser map[43] as fold change over background using bedGraph tracks generated using the MACS2 bdgcmp function with this parameter: -m FE.

To identify differentially accessible regions (DARs), Diffbind v2.10.0[16] was used on the set of ATAC peaks (IDR < 0.05) with these parameters: fragmentSize = 1, summits = 0. ATAC peaks with FDR < 0.05 were considered as significantly differentially accessible regions and used for generating a volcano plot and heatmap comparing Sensitized and Resolved samples. Signal profiling of these ATAC peaks (FDR <0.05) along with their neighboring regions were performed using deeptools[44]. Functional annotation of peaks (GO biological process) and peak-gene association were done with GREAT using the default "basal plus extension" parameter[17]. Sensitized (fc > 1.5) and Resolved-specific DARs (fc < -1.5) were separately analyzed and top 15 enriched pathways were shown in Fig. 3E-F.

Immunoblotting

Cells were lysed with cell lysis buffer (9803S, Cell Signaling) according to the manufacturer's instructions. Rapid Gold BCA protein assay kit was used to determine protein concentrations in the cell lysate (A53225, Thermo Scientific). Equal amounts of protein were separated by SDS-PAGE and transferred to a nitrocellulose membrane. Membranes were incubated overnight with antibodies against Caspase 1 (AG-20B-0042-C100, AdipoGen) and β-actin (MA5-15739, Invitrogen). Corresponding secondary antibodies conjugated with horseradish peroxidase in combination with enhanced chemiluminescence reagent (Amersham, RPN2209) were used to visualize protein bands.

Quantification and statistical analysis

Statistics were performed in GraphPad Prism v8.3.0. For the cell size differences in confocal images and RT-qPCR, pairwise comparisons were performed with the Mann–Whitney U test (two-tailed) or unpaired Student's t test. A value of $P < 0.05$ was considered to be statistically significant.

Data and Materials availability

The authors declare that the data supporting the findings of this study are available within the paper and its Supplementary Information and are also available from the corresponding author upon request. RNA-seq and ATAC-seq data that support the findings of this study have been deposited at NCBI under BioProject ID no.

Method References

28 Chen, S. L. *et al.* Positive selection identifies an in vivo role for FimH during urinary tract infection in addition to mannose binding. *Proc Natl Acad Sci U S A* **106**, 22439-22444, doi:10.1073/pnas.0902179106 (2009).

29 Mulvey, M. A., Schilling, J. D. & Hultgren, S. J. Establishment of a persistent Escherichia coli reservoir during the acute phase of a bladder infection. *Infect Immun* **69**, 4572-4579, doi:10.1128/IAI.69.7.4572-4579.2001 (2001).

30 Wright, K. J., Seed, P. C. & Hultgren, S. J. Uropathogenic Escherichia coli flagella aid in efficient urinary tract colonization. *Infect Immun* **73**, 7657-7668, doi:10.1128/IAI.73.11.7657-7668.2005 (2005).

31 Moon, C., VanDussen, K. L., Miyoshi, H. & Stappenbeck, T. S. Development of a primary mouse intestinal epithelial cell monolayer culture system to evaluate factors that modulate IgA transcytosis. *Mucosal Immunol* **7**, 818-828, doi:10.1038/mi.2013.98 (2014).

32 Pfaffl, M. W. A new mathematical model for relative quantification in real-time RT-PCR. *Nucleic Acids Res* **29**, e45, doi:10.1093/nar/29.9.e45 (2001).

33 Shishkin, A. A. *et al.* Simultaneous generation of many RNA-seq libraries in a single reaction. *Nat Methods* **12**, 323-325, doi:10.1038/nmeth.3313 (2015).

34 Bhattacharyya, R. P. *et al.* Simultaneous detection of genotype and phenotype enables rapid and accurate antibiotic susceptibility determination. *Nat Med* **25**, 1858-1864, doi:10.1038/s41591-019-0650-9 (2019).

35 Trapnell, C., Pachter, L. & Salzberg, S. L. TopHat: discovering splice junctions with RNA-Seq. *Bioinformatics* **25**, 1105-1111, doi:10.1093/bioinformatics/btp120 (2009).

36 Anders, S., Pyl, P. T. & Huber, W. HTSeq--a Python framework to work with high-throughput sequencing data. *Bioinformatics* **31**, 166-169, doi:10.1093/bioinformatics/btu638 (2015).

37 Patro, R., Duggal, G., Love, M. I., Irizarry, R. A. & Kingsford, C. Salmon provides fast and bias-aware quantification of transcript expression. *Nat Methods* **14**, 417-419, doi:10.1038/nmeth.4197 (2017).

38 Love, M. I., Huber, W. & Anders, S. Moderated estimation of fold change and dispersion for RNA-seq data with DESeq2. *Genome Biol* **15**, 550, doi:10.1186/s13059-014-0550-8 (2014).

39 Lee, H. J. *et al.* Regenerating zebrafish fin epigenome is characterized by stable lineage-specific DNA methylation and dynamic chromatin accessibility. *Genome Biol* **21**, 52, doi:10.1186/s13059-020-1948-0 (2020).

40 Langmead, B. & Salzberg, S. L. Fast gapped-read alignment with Bowtie 2. *Nat Methods* **9**, 357-359, doi:10.1038/nmeth.1923 (2012).

41 Zhang, Y. *et al.* Model-based analysis of ChIP-Seq (MACS). *Genome Biol* **9**, R137, doi:10.1186/gb-2008-9-9-r137 (2008).

42 Landt, S. G. *et al.* ChIP-seq guidelines and practices of the ENCODE and modENCODE consortia. *Genome Res* **22**, 1813-1831, doi:10.1101/gr.136184.111 (2012).

43 Zhou, X. *et al.* The Human Epigenome Browser at Washington University. *Nat Methods* **8**, 989-990, doi:10.1038/nmeth.1772 (2011).

44 Ramirez, F. *et al.* deepTools2: a next generation web server for deep-sequencing data analysis. *Nucleic Acids Res* **44**, W160-165, doi:10.1093/nar/gkw257 (2016).

Acknowledgements: The authors thank Washington University Center for Cellular imaging (WUCCI) for preparing and imaging scanning electron microscopy samples, which is supported by the Washington University School of Medicine, The Children's Discovery Institute of Washington University and St. Louis Children's Hospital (CDI-CORE-2015- 505) and the Foundation for Barnes-Jewish Hospital (3770). The funders had no role in study design, data collection and analysis, decision to publish, or preparation of the manuscript. We thank Michael Shih for developing Fiji ImageJ macro code for automatic cell size measurement of confocal images and Karen Dodson for editorial assistance.

Funding: This work was supported by a National Institutes of Health (U01AI095542 to SJH and TJH); a National Institutes of Health Mucosal Immunology Studies Team consortium Young Investigator Award (U01 AI0-5776 to TJH); the Washington University Rheumatic Diseases Research Resource-based Center (P30 AR073752, EDOR); McDonnell International Scholars Academy Fellowship at Washington University in St. Louis (to SKR); National Science Foundation (Graduate Research Fellowship #DGE –114395 to VPO), URL: https://www.nsfgrfp.org/. This project was funded with federal funds from the National Institute of Allergy and Infectious Diseases, National Institutes of Health, Department of Health and Human Services, under Grant Number U19AI110818 to the Broad Institute (to JL).

Author Contributions: Conceptualization, SKR, MC, TJH, and S.J.H.; Methodology, SKR, TS, TW, TJH, and SJH; Investigation, SKR, HJL, JL, VPO, and TJH; Formal Analysis, SKR, HJL, BO, VPO, LY, and EDOR; Writing-Original Draft, SKR; Writing-Review & Editing, SKR, HJL, BO, VPO, SE, AOA, TJH, and SJH; Visualization, SKR, HJL, BO, and VPO; Funding Acquisition, TJH, MC, and SJH; Supervision, TJH and SJH.

Competing interests: The authors declare no competing interests.

Additional Information

Supplementary information:

Supplementary Table 1| List of 2880 significantly differentially accessible regions (DARs) between Sensitized and Resolved USCs and their proximal gene names.

Supplementary Table 2| Differentially expressed genes (DEGs) between Sensitized and Resolved differentiated urothelia are visualized as heatmap.

Supplementary Table 3| Key resources and reagents used in this study.

Correspondence and requests for materials should be addressed to S.J.H

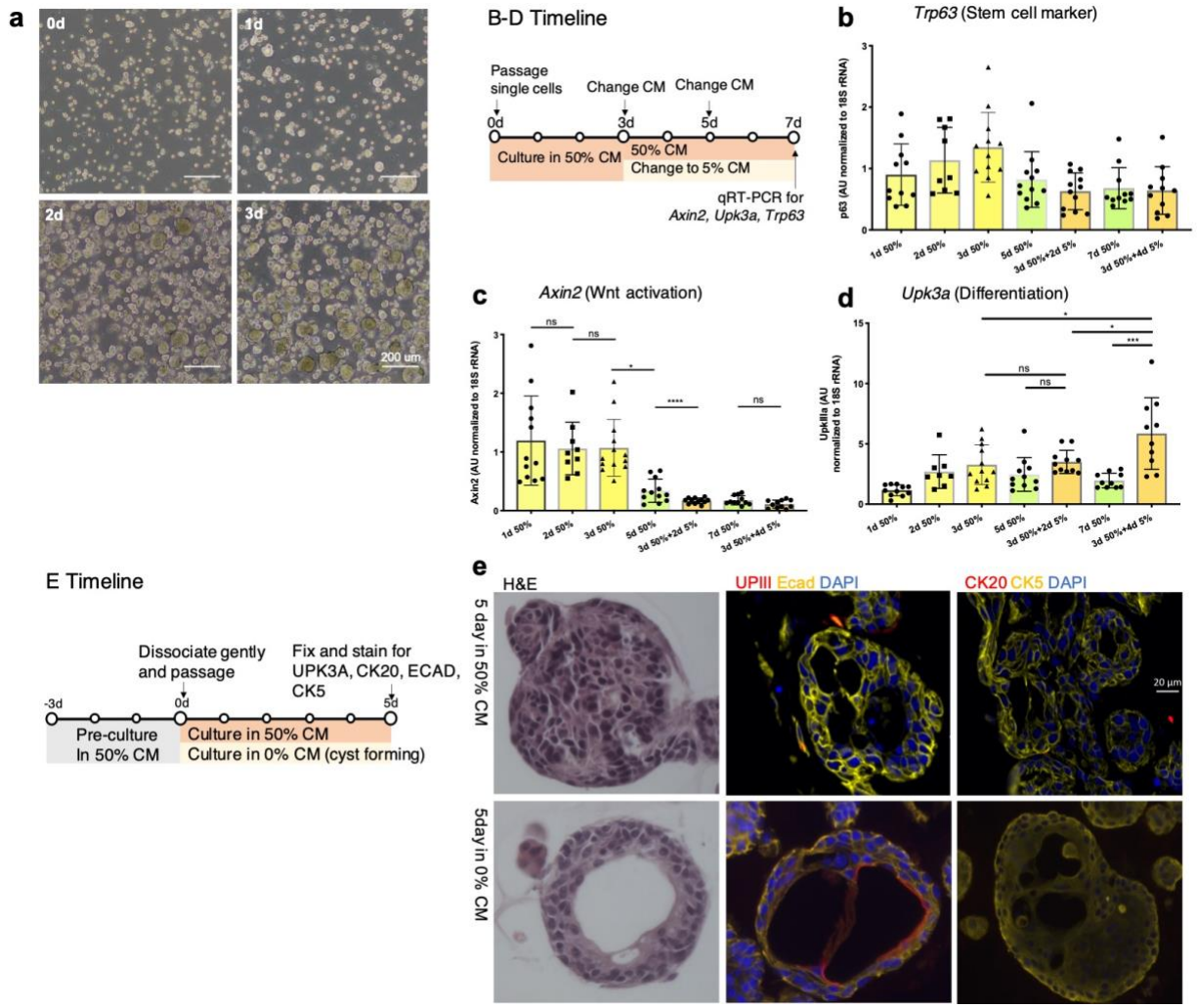

Extended Data Fig. 1| Primary epithelial stem cells possess differentiation potential and stemness, related to Fig. 1. (A) For the cell expansion, dissociated cell aggregates were embedded in fresh matrigel then developed into new spheroids. Urothelial spheroids can be passaged every 3 days using 1:2 – 1:3 dilutions depending on cell density. (B-D) Primary USCs originated from 8 weeks old C3H/HeN mice were cultured in matrigel with 50% CM. After 3 days of culture in 50% CM, media were changed to fresh 50% CM or 5% CM at 3, 5, and 7 days, then RNAs were isolated at 1, 2, 3 (yellow), 5 (green), and 7 days (orange). (B) Gene expressions of *Trp63*, stem cell marker, (C) *Axin2*, Wnt signaling marker, and (D) *Upk3a*, urothelial cell differentiation marker, were measured by qRT-PCR and data are represented as mean ± SD. (E) To culture bladder organoids

826 in matrigel, USCs were pre-cultured in 50% CM for 3 days, gently dissociated, then passaged into
827 fresh matrigel for culture in 50% CM or 0% CM for 5 days, while media were changed every 2
828 days. After 5 day culture, USC spheroids were fixed with 10% neutral buffered formaldehyde
829 (NBF) and prepared for paraffin embedding. The slide with paraffin sections were stained with
830 hematoxylin and eosin (H&E) and immunostained for UPK3A (red), E-cadherin (yellow), and
831 DAPI (blue) or CK20 (red), CK5 (yellow), and DAPI (blue).

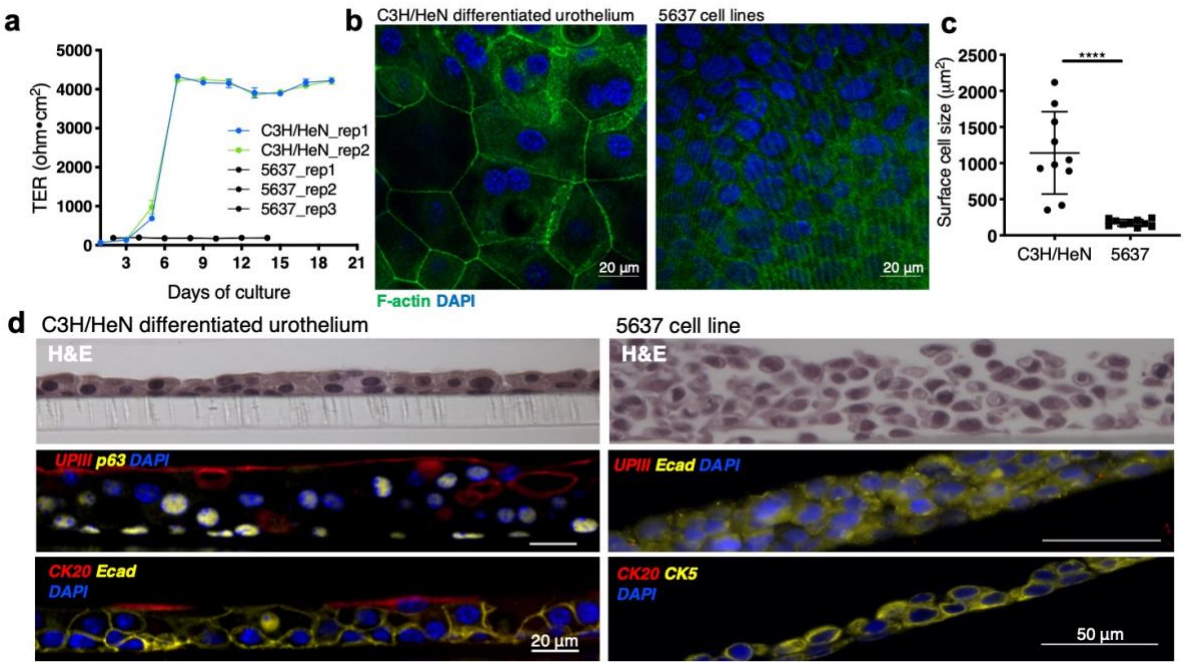

832

833 **Extended Data Fig. 2| The differentiated urothelium better recapitulates the bladder tissue**
834 ***in vivo* compared with human bladder carcinoma cell line, 5637, related to Fig. 1.** (A) Primary
835 C3H/HeN urothelial cells and 5637 cells were cultured in Transwells for 2-3 weeks and
836 transepithelial electrical resistance (TER) of Transwells were measured every 2 days before media
837 change. (B) Whole mount urothelium of both cells were also fixed and stained for confocal
838 staining; F-actin (green) and nuclei (blue). (C) Surface cell size of each primary C3H/HeN
839 urothelial cell and 5637 cell culture was measured using confocal images. Data are represented as
840 mean ± SD. (D) The Transwell cultures of both C3H/HeN and 5637 cells were fixed, cut into slices
841 and then processed for paraffin embedding. Histologic sections were cut and stained with H&E or
842 immunostained for UPK3A (red), CK20 (red), E-cadherin (yellow), CK5 (yellow), Trp63
843 (yellow), and DAPI (blue).

844

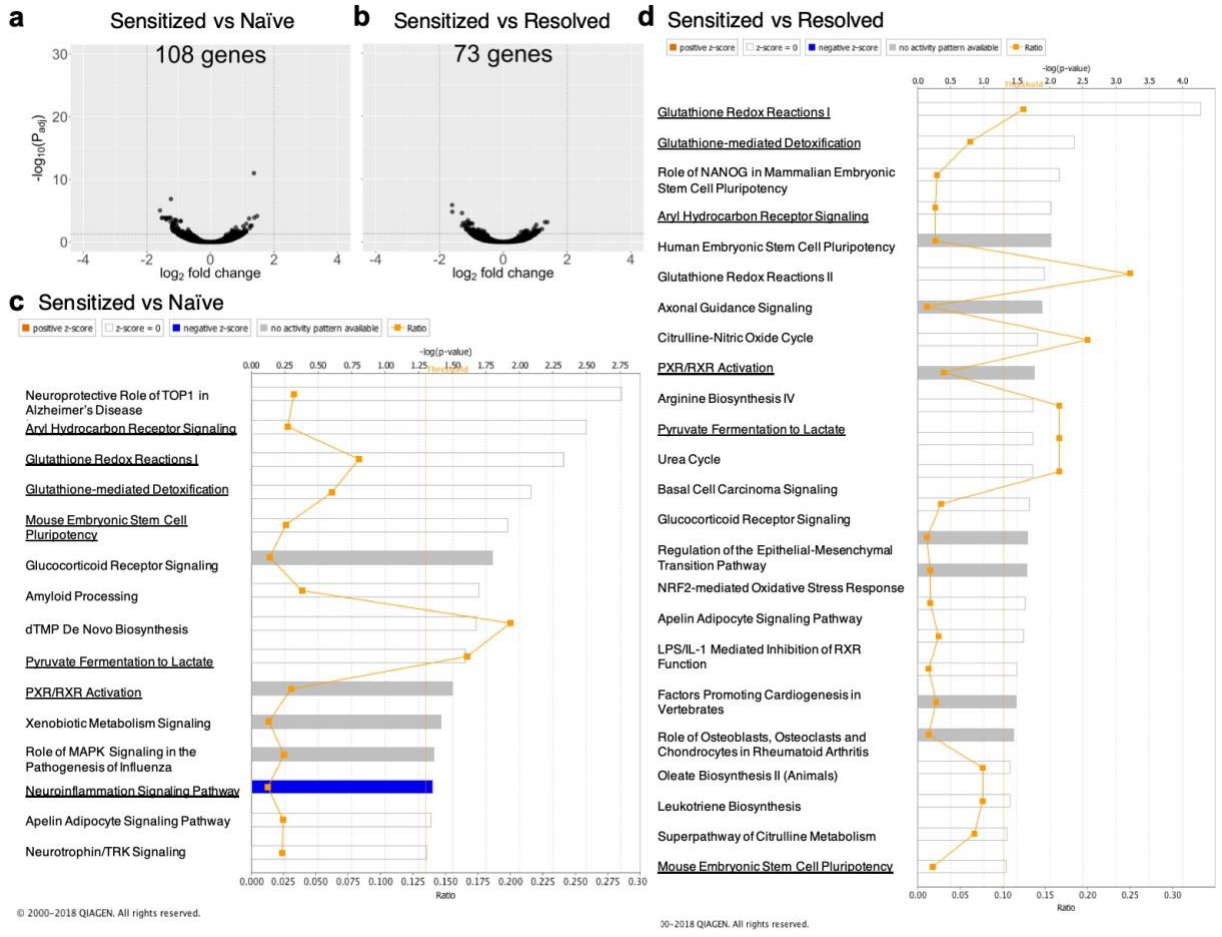

Extended Data Fig. 3| RNA-seq of primary USCs originated from convalescent mice revealed that sensitized USCs maintain differential gene expressions after several passages, related to Fig. 3. RNAs were isolated from Naïve, Resolved, and Sensitized USCs, then analyzed by RNA-seq and performed differential analysis. 108 and 73 genes were significantly differentially expressed in Sensitized USCs relative to (A) Naïve and (B) Resolved USCs (P-adj < 0.05). Enriched pathways in Sensitized compared with (C) Naïve and (D) Resolved USCs are listed here. Overlapping pathways in both analyses are underlined, which are related with apoptosis, ROS response, and immune response.

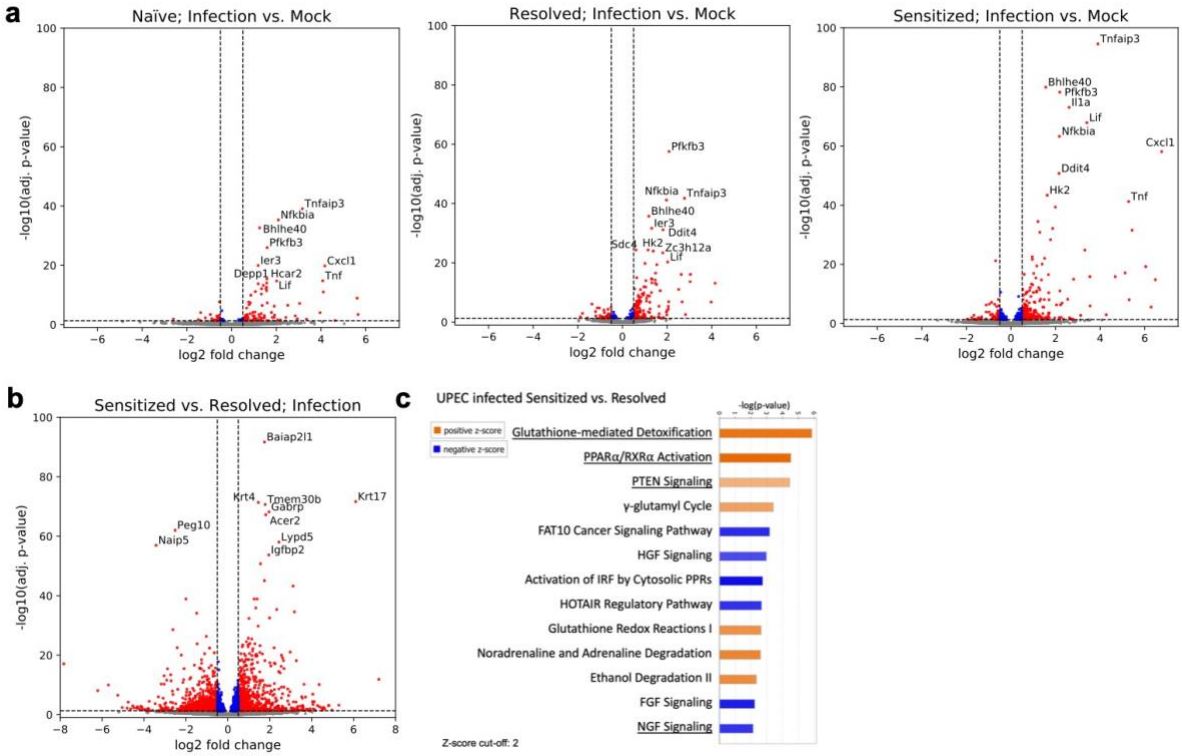

Extended Data Fig. 4| Differential transcriptomics of differentiated urothelia originating from convalescent mice recapitulate *in vivo* studies, related to Fig. 4. RNA-seq data of UTI89 infected and mock-infected differentiated urothelia was used here to perform differential analysis. (A) Volcano plot comparing UPEC infected vs. mock-infected Naïve, Resolved, and Sensitized differentiated urothelia (UPEC infection response). (B) Volcano plot comparing UPEC infected Sensitized vs. Resolved differentiated urothelia was performed. (C) Pathway analysis was used to assess the biological pathways enriched in differentially expressed genes in UPEC infected Sensitized differentiated urothelia relative to Resolved differentiated urothelia, and significance was determined by a right-tailed Fisher's exact test, with P-adjusted <0.05 considered significantly enriched pathways. Shown are selected pathways with z-score > 2 and –log(p-value) > 2 from the specific enriched pathways by Ingenuity Pathway Analysis (IPA).

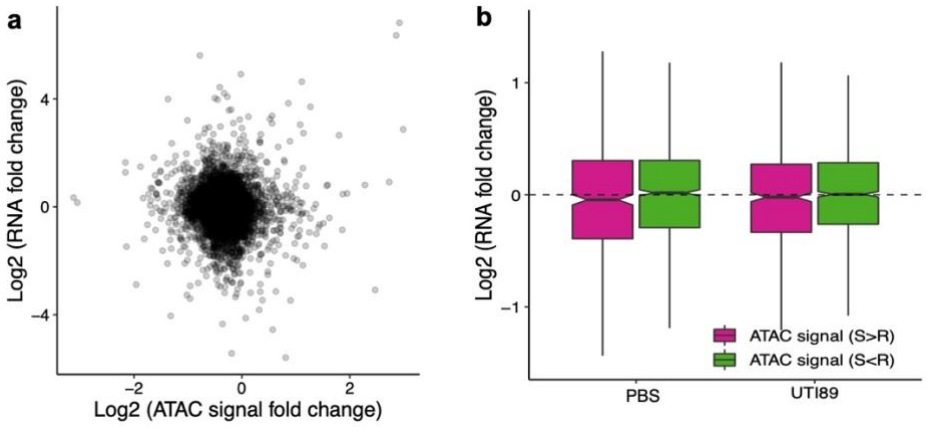

868

869 **Extended Data Fig. 5| Global correlation analysis of RNA-seq and ATAC-seq summary**
870 **statistics showed no significant correlation between transcriptomics and chromatin**
871 **structures, related to Fig. 5.** Correlation analysis of ATAC-seq DARs and RNA-seq DEGs were
872 performed using fold changes of Sensitized vs. Resolved for both DARs and DEGs. (A) Global
873 correlation analysis using all genes are plotted. (B) Relative fold changes of RNA-seq of each
874 mock-infected and UPEC infected are shown. Log2 (RNA fold change) are close to dashed
875 horizontal line, indicating that there is no specific direction of correlation (positive or negative).

Expr Log Ratio (up)		Expr Log Ratio (down)	
Molecules	**Value**	**Molecules**	**Value**
Casp1	6.814	Igf2bp1	-7.498
Gypc	6.592	Olfm4	-6.513
Akr1e2	6.349	Prl2c2 (includes others)	-5.431
Gdf10	6.336	Itga7	-5.298
Rgs9bp	5.604	Ccl5	-5.156
Krt17	5.204	S100a9	-4.553
Ugt8	5.136	A430010J10Rik	-4.460
Stfa1 (includes others)	4.987	Fam221a	-4.342
Ddit4l	4.912	Spp1	-4.340
Adamts5	4.912	Duox2	-4.262

Extended Data Table 1| Top analysis ready molecules from IPA comparing mock-infected Sensitized vs. Resolved differentiated urothelia. "Exp Log Ratio" indicates expression log2 fold change.

Supplementary Files

This is a list of supplementary files associated with this preprint. Click to download.

- SupplementaryTable3.docx
- SupplementaryTable1.xlsx
- SupplementaryTable2.xlsx